

Voltage and temperature effects on the carrier mobility of CuPc organic thin films

F. HIJAZI^{a,b}, N. CHOUEIB^a, H. GHAMLOUCHE^{a,*}, M. YASSINE^a

^aDepartment of Physics, Lebanese University, Beirut, Lebanon

^bXLIM UMR 6172 – Université de Limoges/CNRS, Limoges Cedex, France

Voltage and temperature dependence of the carrier mobility of CuPc organic semiconductor is presented using impedance spectroscopy measurements and current–voltage characteristics. Through current–voltage curve, four distinct regions are identified. At low bias voltage an ohmic region is observed (zone 1). By increasing the voltage, a space charge limited region appears due to the existence of trap states (zone 2). A further increase in the voltage leads to a traps filled limit region (zone 3). The last observed region is a trap-free square one, where the current rises linearly (zone 4). From current-voltage curve, V_{Ω} is found (0.18V) and used to calculate the carriers' concentration ($2 \times 10^{20} \text{ e}\cdot\text{m}^{-3}$). From impedance spectroscopy measurements, the dependence of the mobility on temperature permits the identification of two types of activation energies. Furthermore, the variation of the mobility as a function of the voltage doesn't obey completely the Poole–Frenkel's law, since a slight deviation from linearity above certain applied voltage is observed.

(Received January 18, 2019; accepted August 20, 2019)

Keywords: Carrier mobility, CuPc, Organic thin films, Impedance spectroscopy, Current–voltage characteristics

1. Introduction

The recently discovered cells based on inorganic or organic semiconductors commonly referred to as 'bulk' junctions due to their three-dimensional structure, are very attractive alternatives which offer the prospect of very low cost fabrication [1]. The introduction of semi-conductor polymers and organic pigments opened the door for the incorporation of organic semiconductors in the manufacture of solar cells [2]. There has been tremendous effort to develop organic solar cells within the last three decades. Organic photovoltaic (OPV) cells have attracted remarkable interest as a possible alternative to conventional inorganic photovoltaic technologies. Some key advantages for OPVs are that they are inherently inexpensive and they have low environmental impact during manufacturing and operations [3, 4]. These reasons have led to the push of organic solar cells.

Charge carriers are photogenerated, with very different spatial distribution, in conventional inorganic and OPV cells. This leads to a fundamental difference between the mechanisms. Due to the low dielectric constant in organic semiconductors, the coulomb interaction between an electron and a hole is very high, so the exciton (electron–hole pair) is the product of the light absorption [5]. These excitons are not easily dissociated; they require an input energy of $\sim 100 \text{ meV}$, which is not achieved at room temperature as in the case of inorganic semiconductors [2]. Due to the high degree of disorder present in many organic solids, charge carrier mobility is generally low.

To further improve the performance of organic devices (i.e. the efficiency) and to understand the device physics, information about transport processes is of fundamental importance [6]. Impedance spectroscopy (IS) is one of several techniques that can be used to elaborate the transport parameters such as mobility, localized states

distributions and deep trapping lifetimes. From the arrangement of the elements in the equivalent circuit, one can draw implications about the mechanisms taking place in the cell. In addition, from the numerical values of the resistors and capacitors needed to produce a response similar to the actual PV cell, the numerical values of the main transport parameters can be deduced.

One of the most popular organic semiconductors is phthalocyanine (Pc). This compound was traditionally used as dyes and pigments. In addition, Pc presents a special interest due to its low cost and potentially high photoelectronic properties [7]. Copper phthalocyanine (CuPc), was reported to have high electron mobility where electrons are the dominant carriers in transport, in contrast to most organic materials [8].

CuPc was used in many experiments as an organic active layer. Using IS and current–voltage (J–V) analysis on CuPc diodes, the conductivity was calculated and equivalent circuits were modeled [9]. Using optical and capacitance spectroscopy, energy gap of CuPc device was calculated, and from J–V analysis permittivity was calculated and defect distribution of states was studied [7]. An exponential trap distribution was revealed from the study of CuPc/n–Si hybrid solar cells [10]. Observations of two regimes while varying the temperature and bias voltage were discussed in [11]. At low bias voltage and high temperature, the results are best explained with Poole–Frenkel type transport model, while at high bias voltage and low temperature, space charge limited current controlled by an exponential distribution of traps dominates the transport. Electrically active defects were investigated with space charge capacitance spectroscopy, as function of temperature and frequency [11].

The motivation of this work is to further investigate the transport mechanisms in CuPc semiconductor. In order to do that, we have prepared samples of CuPc that is

sandwiched between two electrodes, Al (aluminum) and ITO (Indium Tin Oxide). Using IS and J–V curves, mobility will be calculated as functions of the bias voltage and temperature. The data obtained from these two techniques will be useful to study the transport mechanisms as functions of the applied bias voltage and temperature. From J–V curves, the applicability of Poole–Frenkel transport model will be explored. Whereas from IS curves, the temperature dependence of the carrier mobility, at zero applied bias, and transport regimes will be investigated.

2. Experimental

In all performed measurements, samples in sandwich form were used. The organic film was deposited between two electrodes; the bottom one was an Indium–Tin–Oxide (ITO) layer, whereas the top electrode was from aluminum (Al).

The ITO layer was deposited on a glass substrate and had a thickness of 150 nm and a transmittance of the order of 89 % in the visible light. The substrate had an area of 144 mm² and a thickness of 1.1 mm.

The preparation of the CuPc and the cathode (Al) was done by thermal evaporation under vacuum. The thicknesses of the CuPc film and the cathode were of 25 nm and 100–200 nm, respectively.

The impedance spectroscopy technique consisted of: a) Impedance analyzer (HP 4284A) with a frequency range of 20 Hz–1 MHz. b) Keithley multimeter 199 to determine the temperature of the sample. c) A power supply to heat the sample.

The setup of the experiment gave us the magnitudes of the capacitance C and conductance G . The real (ϵ') and imaginary (ϵ'') parts of the permittivity ϵ were derived from the obtained values of C and $G = 1/R$ using the following equations:

$$\epsilon' = C \frac{d}{A} \quad (1)$$

$$\epsilon'' = \frac{G}{\omega(A/d)}, \quad (2)$$

where d and A are the thickness and area of the active layer, respectively. The real and imaginary parts of the impedance Z were derived from C and G using the following equation:

$$Z(\omega) = \left[R_s + \frac{R}{1 + (\omega/\omega_0)^2} \right] - j \left[\frac{R(\omega/\omega_0)}{1 + (\omega/\omega_0)^2} \right] \\ = \text{Re}(Z) + j\text{Im}(Z) \quad (3)$$

where ω is the angular frequency of the AC excitation, and ω_0 is the proper angular frequency of the circuit ($\omega_0 = 1/RC$). According to this equation, a plot of $-\text{Im}(Z)$ as a function of $\text{Re}(Z)$ would give a semicircle where its diameter represents the resistance of the device under test. This plot is well known as Cole–Cole plot.

In order to measure the current (or current density) as a function of an applied voltage (or electric field) the following equipment were used: a) Electrometer Keithley 617 (USA) to measure the current along the sample after applying the voltage. b) A voltage source: Thurlby Thunder Instruments (TTI) of type PL330P (USA). This source is used to apply a voltage across the sample.

3. Results

Fig. 1 shows the current density as a function of the bias voltage. Four different zones are identified; each corresponds to a different behavior of the transport properties of the electrons in the cell.

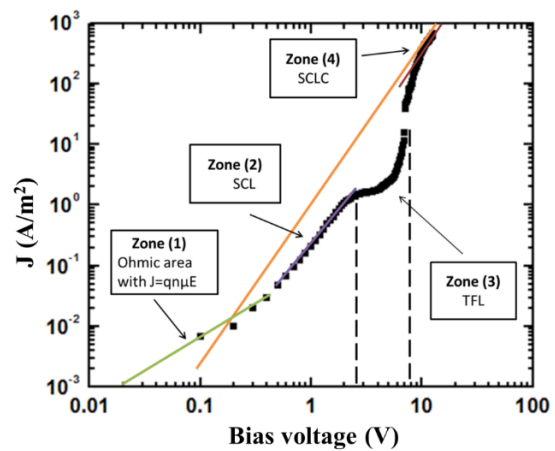


Fig. 1. Current density as a function of voltage. Four zones are shown: a) Ohmic regime (zone 1); b) SCL regime (zone 2); c) TFL regime (zone 3); d) SCLC regime (zone 4)

In Fig. 2 Cole–Cole plot of the device at several bias voltages (0–6 V) is shown.

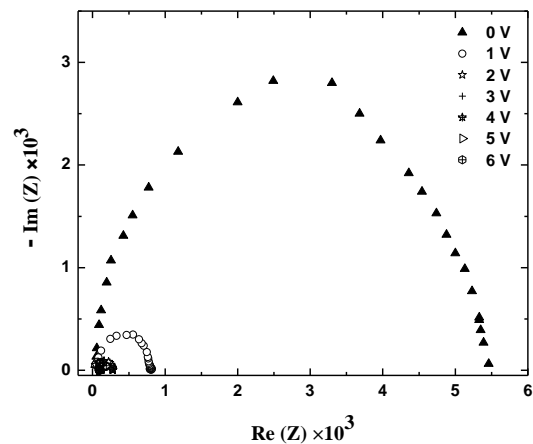


Fig. 2. $\text{Im}(Z)$ as a function of $\text{Re}(Z)$ for different bias voltages (0–6 V). A shift to lower frequencies of the semicircles is observed as the bias voltage is increased

Fig. 3 shows relative imaginary permittivity ϵ_r'' as a function of the frequency ω at different bias voltages (0–6 V).

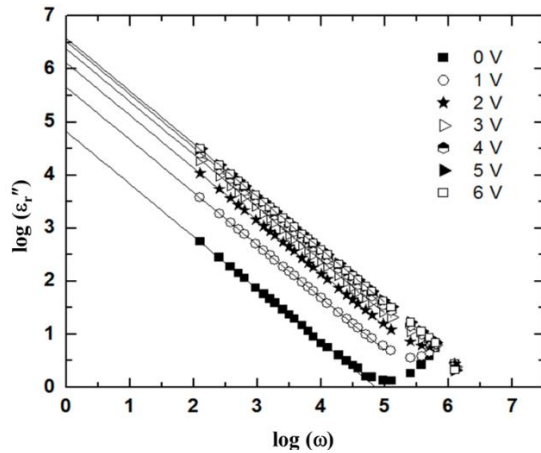


Fig. 3. $\log(\epsilon_r'')$ as a function of $\log(\omega)$ for different bias voltages (0–6 V). An increase of the conductivity (γ) is observed as the bias voltage is increased

The carriers' mobility as a function of the square root of the bias voltage is shown in Fig. 4.

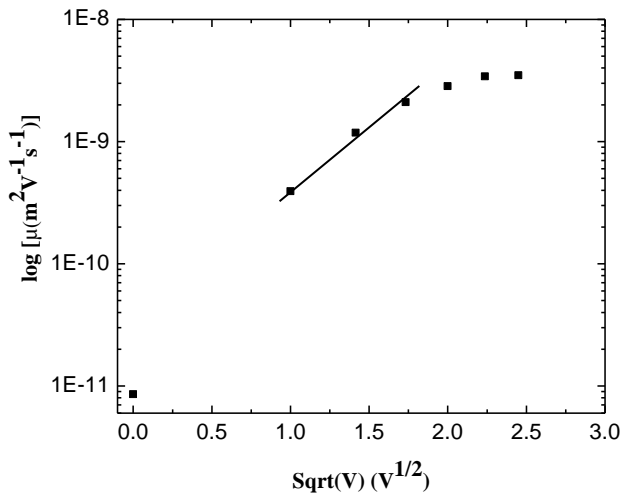


Fig. 4. $\log(\mu)$ as a function of $\text{sqrt}(V)$. A clear deviation from linearity is observed at high voltages

Fig. 5 exhibits the Cole–Cole plot of the device at several temperatures (173–373 K, for a step of 20 K).

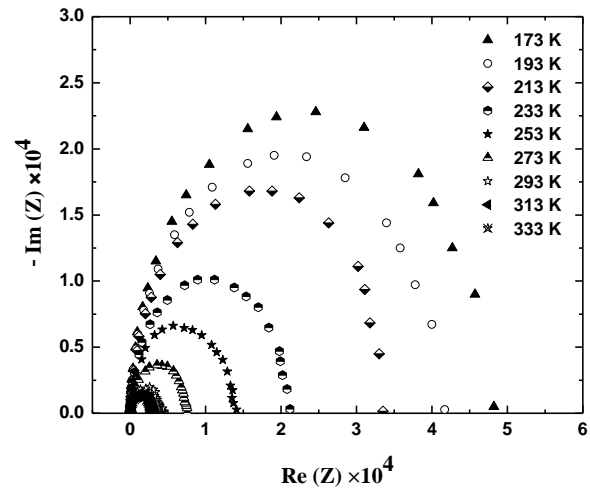


Fig. 5. $\text{Im}(Z)$ as a function of $\text{Re}(Z)$ at different temperatures (173 K–373 K). A shift to lower frequencies of the semicircles is observed as the temperature is increased

In Fig. 6 the relative imaginary permittivity ϵ_r'' as a function of frequency for several temperatures (173–373 K, for a step of 40 K) is plotted.

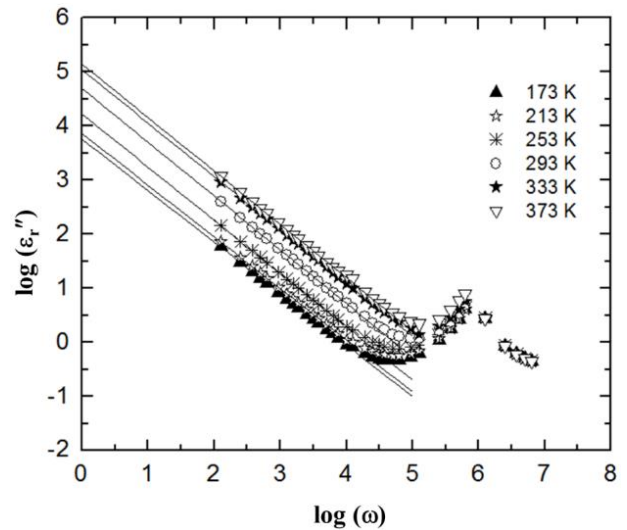


Fig. 6. $\log(\epsilon_r'')$ as a function of $\log(\omega)$ for different temperatures (173 K–373 K). An increase of the conductivity (γ) is observed as the temperature is increased

Fig. 7 shows the variation of the carriers' mobility as a function of the inverse of temperature T .

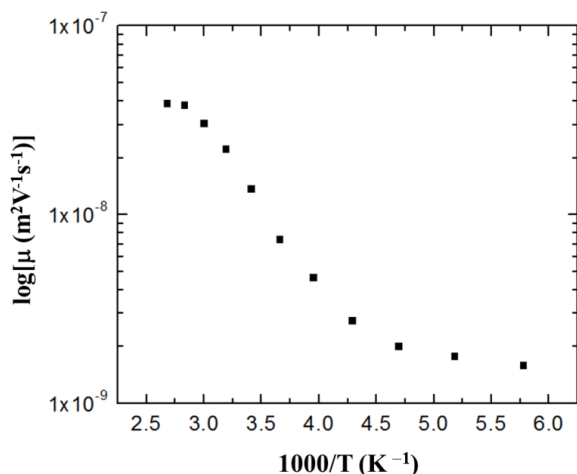


Fig. 7. $\log(\mu)$ as a function of $1000/T$. Two different behaviors are observed at high and low temperatures

The frequency ω_0 and the relative imaginary permittivity ϵ_r'' as a function of the inverse of temperature T are plotted in Fig. 8. The frequency ω_0 is extracted from each curve of Fig. 5, where $-\text{Im}(Z) = \text{Re}(Z)$ (i.e. at the maximum of the semicircle). The solid lines represent the slopes of two different regimes. These two slopes are the same for the two curves.

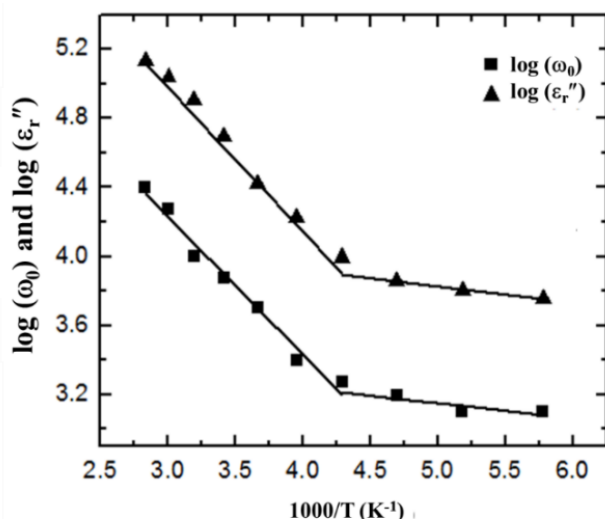


Fig. 8. $\log(\omega_0)$ and $\log(\epsilon_r'')$ as a function of $1000/T$. Shallow and deep traps are detected with activation energies of 8.1 ± 0.4 meV and 72.1 ± 3.60 meV, respectively

4. Analysis

Before starting the analysis, the structural properties of CuPc are presented. The molecular structure of CuPc is schematically shown in Fig. 9. It has a planar structure with D_{4h} point symmetry. The molecule consists of the central Cu atom, which is surrounded by four pyrrole nitrogen atoms (N1); four other nitrogen atoms (N2) and 32 carbon

atoms—the pyrrole (C1) and the benzene (C2, C3 and C4). [12]

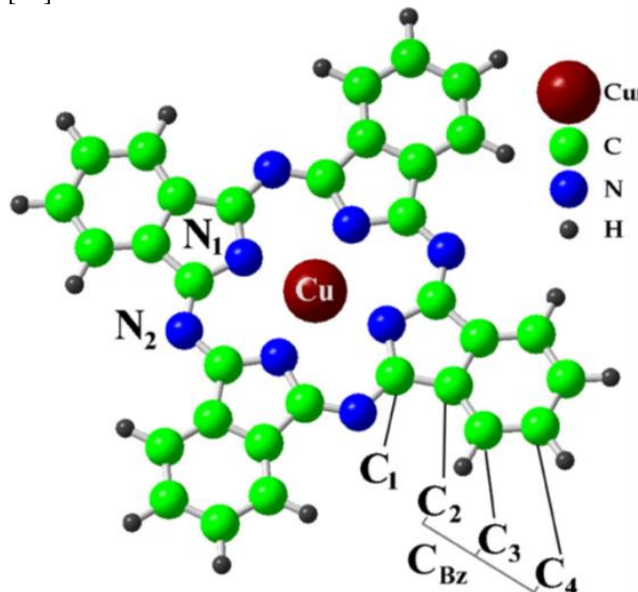


Fig. 9. Schematic representation of the molecular structure of the CuPc molecule

Regarding the electronic properties of CuPc studied using photoemission spectroscopy [13] the onset of the CuPc valence band, which corresponds to emission from the highest occupied molecular orbital HOMO is found at 1.15 eV binding energy. The work function is defined as the distance between the Fermi and vacuum levels. In pristine CuPc the Fermi level lies in the energy gap of CuPc. The band gap of CuPc is about 2.3 eV. From these details, it follows that the Fermi energy of CuPc lies in the middle of a HOMO-LUMO gap, which confirms that pure CuPc without any impurities could be regarded as an intrinsic semiconductor.

In Fig. 1, the first and the last zones (1 and 4) correspond to an ohmic conduction that is not involving any traps. The second zone corresponds to the space current limited (SCL) conduction due to trap effects. The third zone shows traps filled limit (TFL) law, where all the traps are occupied. The intersection of the two slopes of the ohmic regions corresponds to V_Ω ($\sim 0.18 \pm 0.01$ V). The behavior of the J–V curve in this figure confirms the theoretical studies concerning the transport mechanisms in organic semiconductors [14]. Recent studies on Au/n–Si/CuPc/Au heterojunction [10] have shown a similar behavior where, three zones have been identified, whereas in our case four zones can be distinguished. The additional zone is related to TFL mechanism, which has been obtained and identified previously in Alq3 [15]. Comparing our results to a recent study [16], we notice a similar behavior of J–V curve, where the slope of the ohmic zone ($J \propto V$) is found to be unity, while that of the second zone ($J \propto V^2$) is found to be 2. Furthermore, V_Ω , which was deduced previously, enables us to calculate the concentration of the carriers n_0 and the mobility μ [15].

$$n_0 = \frac{9 \varepsilon_0 \varepsilon_r}{8 q d^2} V_{\Omega} = \frac{9}{8} \frac{8.85 \times 10^{-12} \times 3.4}{1.6 \times 10^{-19} \times 6.25 \times 10^{-16}} \times 0.18 = (6.09 \pm 0.3) \times 10^{22} \text{ e} \cdot \text{m}^{-3} \quad (4)$$

$$\mu = \frac{\gamma_0}{q n_0} = \frac{5.98 \times 10^{-7}}{1.6 \times 10^{-19} \times 6.09 \times 10^{22}} = (6.14 \pm 0.3) \times 10^{-11} \text{ m}^2 \cdot \text{V}^{-1} \cdot \text{S}^{-1}, \quad (5)$$

where, q is the elementary charge, d (25 nm) is the thickness of the active layer, ε_r (3.4) the relative permittivity [17]. In Fig. 2, on one hand, the minimum value of $\text{Re}(Z)$ (corresponding to the highest frequency) shows that there is a negligible series resistance R_s ($\sim 0 \Omega$). On the other hand, the diameter of each semicircle corresponds to the resistance R that is parallel to the capacitor. Therefore, the equivalent circuit becomes simply a single capacitor C parallel to the resistor R . Moreover, as the DC bias voltage increases the semicircles shrink.

In Figs. 3 and 6, based on the following equation, one can find the y-intercept (extrapolation of the curve to $\log \omega = 0$), which directly leads to γ_0 ($\varepsilon'' = \gamma_0$):

$$\log \varepsilon'' = \log \gamma_0 - \log \omega \quad (6)$$

For example, at zero bias, $\varepsilon''/\varepsilon_0 = (6.76 \pm 0.33) \times 10^4$, so that: $\varepsilon'' = (5.98 \pm 0.30) \times 10^{-7}$ and consequently $\gamma_0 \approx (6.0 \pm 0.3) \times 10^{-7} \text{ ohm}^{-1} \cdot \text{m}^{-1}$.

In addition, the behavior of the curves in these two figures confirms the theoretical results in what concerns the two regions of low and high frequency [11]. Region 1 (low frequency) is a straight line (of slope ~ -1), where ε'' depends on temperature and frequency according to Eq. (6). In region 2 (high frequency), ε'' depends only on frequency according to the following equation [11]:

$$\log \varepsilon_r'' = \log \frac{(\varepsilon_s - \varepsilon_{\infty})}{\tau} - \log \omega \quad (7)$$

In Fig. 4, the variation of $\log \mu$ with respect of \sqrt{V} is usually analyzed using Poole–Frankel expression. In the 1990s, the field-dependent mobility model was initially proposed by Bessler, as the result of assuming hopping transport in a gaussian density of states (DOS). Random walk with Monte Carlo simulations yielded to the well-known Poole–Frenkel expression:

$$\mu = \mu_0 \exp(\alpha \sqrt{E}) \quad (8)$$

in which μ_0 is the zero-field mobility for a particular carrier species in the material, E is the electric field, and α is a temperature-dependent but assumed to be field independent parameter [18, 19].

The Poole–Frenkel expression is typically used to study the field dependence of mobility at constant temperature. In most cases, positive field dependence ($\alpha >$

0) is observed. Since the temperature is constant, one should expect that the parameter α to be independent of the applied electric field. In this study, a nonlinear behavior of the variation of $\log \mu$ with respect to \sqrt{V} has been observed, in contrast to the results found in recent studies [16]. At low electric fields, there is no sufficient energy to increase the mobility (i.e. it is independent of E). For intermediate values of E , Poole–Frenkel model is valid, but at high fields the conductivity saturates. Several authors have obtained a similar behavior, but for different materials, as cited in [20, 21].

In Fig. 5, as the temperature increases, the radii of the semicircles decrease. This is expected since the conductivity increases with temperature.

In Fig. 7, according to Eq. (6) for $\omega = 1$, and by using Eq. (5), $\log \varepsilon'' = \log(n_0 q) + \log \mu$. Therefore, the behavior of $\log \varepsilon''$ becomes similar to the behavior of $\log \mu$, as shown in Fig. 8. In these two figures, the behavior of the curves shows that there are two types of traps in this material; shallow and deep. From these slopes one can calculate the activation energies of the traps by following Gill's expression that leads to the Arrhenius-like behavior:

$$\mu = \Gamma \exp\left(\frac{E_t}{k_B T}\right), \quad (9)$$

where E_t is the activation energy of trap states and k_B is the Boltzmann constant and Γ is the mobility at very high temperature [22].

The deep traps have activation energy of 72.1 ± 3.60 meV, whereas that of shallow traps it is 8.1 ± 0.4 meV. Results on CuPc [7] have identified only deep traps of 320 meV. However, both types of traps have been identified for other materials [20]. Up to our knowledge, the detection of two types of traps in CuPc is observed for the first time.

5. Conclusions

CuPc organic semiconductor was used as an active layer between Al and ITO electrodes. Transport mechanisms were studied using current–voltage (J–V) characteristics and impedance spectroscopy measurements. Through J–V curve, four distinct zones were identified. At low bias voltage, an ohmic zone was observed due to the ohmic contact. By increasing the voltage, SCL zone appears due to the existence of trap states. TFL zone then was observed, where all traps are filled. The last zone was a Trap-free square one, where the current rises linearly (ohmic zone). Using the J–V curve, V_{Ω} was found to be 0.18V, then the concentration of carriers was calculated, $n_0 = 6.09 \times 10^{20} \text{ e} \cdot \text{m}^{-3}$. From impedance spectroscopy measurements, mobility was determined while varying temperature and voltage. At zero bias voltage, mobility was calculated ($\mu = 6.14 \times 10^{-11} \text{ m}^2 \cdot \text{V}^{-1} \cdot \text{s}^{-1}$). The dependence of the mobility on temperature permitted the identification of two types of activation energies, one related to shallow traps, while the other corresponds to deep traps. Shallow traps have activation energy of 8.1 meV, while deep traps have 72.1 meV. Furthermore, the variation of mobility as a

function of \sqrt{V} is deduced from impedance spectroscopy measurements; it doesn't obey completely the Poole-Frenkel law since a slight deviation from linearity above certain applied voltage was observed. At low electric fields, there is no sufficient energy to increase the mobility (i.e. it is independent of E). For intermediate values of E , Poole-Frenkel model is valid, but at high fields the conductivity saturates.

Further investigations will be done on CuPc and compare the results with other organic compounds in order to be able to select appropriate compounds suitable for photovoltaic devices.

Acknowledgments

This project has been funded with support from the Lebanese University (4/6081 and 4/6132). The authors would like to thank the Lebanese University for this support.

References

- [1] M. Gratzel, *Philos. T. R. Soc. A* **365**(1853), 993 (2007).
- [2] M. B. Askari, *J. Renew. Sustain. Energy* **3**(3), 53 (2014).
- [3] S. E. Shaheen, D. S. Ginley, G. E. Jabbour, *MRS Bull.* **30**, 10 (2005).
- [4] H. Hoppea, N. S. Sariciftci, *J. Mater. Res.* **19**, 7 (2004).
- [5] B. A. Gregg, M. C. Hanna, *J. Appl. Phys.* **93**, 3605 (2003).
- [6] S. Baranowski, *Charge transport in disordered solids with applications in electronics*, Wiley-Chichester (2006).
- [7] F.T. Reis, D. Mencaragliaa, S. O. Saada, I. Seguyb, M. Oukachmihb, P. Jolinatb, P. Destruelb, *Synth. Met.* **138**, 33 (2003).
- [8] Y. Yanting, Y. Yanming, W. Fugen, W. Zhigang, *Solid State Commun.* **148**, 559 (2008).
- [9] C.-H. Kim, H. Hlaing, S. Yang, Y. Bonnassieux, G. Horowitz, I. Kymissis, *Org. Electron.* **15**(8), 1724 (2014).
- [10] L. Yiting, L. Aimin, H. Zengquan, L. Weifeng, Q. Fen, *J. Phys. Chem. Solids* **73**, 626 (2012).
- [11] F. T. Reis, D. Mencaraglia, S. Ould Saad, I. Séguy, M. Oukachmih, P. Jolinat, P. Destruel, *Synthetic Met.* **138**, 33 (2003).
- [12] V. Yu. Aristov, O. V. Molodtsova, V. Maslyuk, D. V. Vyalikh, V. M. Zhilin, Yu. A. Ossipyan, T. Bredow, I. Mertig, M. Knupfer, *Applied Surface Science* **254**, 20 (2007).
- [13] F. Evangelista, *J. Chem. Phys.* **126**, 124709 (2007).
- [14] S. Takeshita, PhD thesis, Modelling of space-charge-limited current injection incorporating an advanced model of the Poole-Frenkel effect, Clemson University, South Carolina State, (2008).
- [15] A. Moliton, W. Rammal, B. Lucas, *Eur. Phys. J. Appl. Phys.* **33**, 175 (2006).
- [16] Z. Ahmad, M. H. Sayyad, Kh. S. Karimov, *J. Semicond.* **31**(7), 074002-(1-4) (2010).
- [17] N. Shi, R. Ramprasad, *J. Appl. Phys.* **89**, 102904 (2006).
- [18] H. Bassler, *Phys. Status Solidi B* **175**, 15 (1993).
- [19] P. M. Borsenberger, J. J. Fitzgerald, *J. Phys. Chem.* **97**, 4815 (1993).
- [20] S. Ishihara, H. Hase, T. Okachi, H. Naito, *Thin Solid Films* **554**, 213 (2014).
- [21] L. Li, S. Van Winckel, J. Genoe, P. Heremans, *Appl. Phys. Lett.* **95**, 153301 (2009).
- [22] J. D. Wrigh, *Molecular crystals*, Cambridge University Press, Cambridge, (1995).

*Corresponding author: hassan.ghamlouche@ul.edu.lb